JOURNAL OF GEOPHYSICAL RESEARCH, VOL. 93, NO. B1, PAGES 383–391, JANUARY 10, 1988

Elasticity of Enstatite and Its Relationship to Crystal Structure

THOMAS S. DUFFY[1] AND MICHAEL T. VAUGHAN

Department of Geological Sciences, University of Illinois at Chicago

The nine adiabatic single-crystal elastic moduli of a natural orthopyroxene of enstatite composition ($Mg_{0.94}Fe_{0.06}SiO_3$) have been measured at ambient conditions by Brillouin spectroscopy. The single-crystal elastic stiffnesses in gigapascals (GPa) are c_{11} = 229.3 ± 1.1; c_{22} = 167.0 ± 1.1; c_{33} = 193.9 ± 1.5; c_{44} = 79.7 ± 0.7; c_{55} = 76.1 ± 0.6; c_{66} = 77.1 ± 0.9; c_{12} = 73.6 ± 1.7; c_{13} = 49.8 ± 1.6; and c_{23} = 46.6 ± 1.6. The average Hashin-Shtrikman bulk and shear moduli are 102.2 and 73.9 GPa, respectively. The results of this study are generally consistent with those obtained for other Mg-rich pyroxenes. Some of the individual moduli along the enstatite-ferrosilite join can be related to specific chemical and structural features. The most variable modulus is c_{33}, and it appears to be a complicated function of both chemistry and structure. Its magnitude relative to c_{11} is most easily explained by the presence or absence of more than one tetrahedral chain. For orthopyroxenes of intermediate composition c_{11} is higher than expected, probably due to a combination of the effects of site ordering and impurities in the M1 site. The third longitudinal modulus, c_{22}, is observed to increase linearly as a function of enstatite composition from En_0 to En_{100}. An alternative interpretation for c_{11} and c_{22} is that between $En_{100}$and En_{50}, c_{11} is constant and c_{22} decreases linearly with increasing iron content, while between En_{50} and En_0, c_{11} decreases linearly and c_{22} is constant. The shear and off-diagonal moduli vary nonsystematically but tend to vary in similar ways. With the exception of c_{12}, the averaged moduli also show nonsystematic variations. Cation site ordering appears to strongly affect c_{44}. The modulus c_{11} is also nonsystematic but for reasons which are not obvious. Our results are consistent with the interpretation that the bulk modulus does not vary with composition whereas the shear modulus does so in a linear fashion.

1. INTRODUCTION

1.1 *Importance of Elasticity Data*

Detailed knowledge of the internal structure of the Earth has remained an elusive goal for the Earth sciences. One approach to the problem is to determine the constraints that may be placed on the physical properties of the Earth's interior by comparing observed properties with those obtained by laboratory measurements of relevant materials. For instance, the passage of seismic waves through the Earth reveals information about the elastic properties of the materials composing the Earth's interior. Many authors [e.g., *Weidner*, 1985; *Bass and Anderson*, 1984] have attempted to compare the laboratory-derived elastic properties of proposed mineral assemblages with observed seismic velocities. The success of such modeling depends on an accurate knowledge of the elastic behavior of the proposed minerals. For many important minerals, however, such knowledge is lacking or incomplete. This study represents an attempt to characterize better the elasticity of one important mineral group, orthopyroxenes, by measuring the single-crystal elastic constants of a sample of enstatite composition at ambient conditions by Brillouin spectroscopy.

2. EXPERIMENTAL DETAILS AND RESULTS

2.1 *Sample*

The sample used in this study was taken from a cleavage flake chipped off a larger sample provided by a commercial gem dealer. Its origin is thought to be Tanzania. The cleavage flake was approximately 5 × 3 × 0.5 mm and possessed two excellent cleavages of the form {210}. Optical microscopy revealed that the flake contained a number of small irregularly shaped inclusions of unknown composition. Microprobe analysis (Table 1) showed that the flake was an enstatite of composition $Mg_{0.94}Fe_{0.06}SiO_3$.

In addition to natural growth faces, {001} surfaces were ground flat using a thin section grinder. The grinding process caused the crystal to cleave into a large number of fragments. From these was chosen a high-quality specimen with dimensions of about 0.75 mm × 0.25 mm × 0.075 mm and displaying {001}, {010}, {100}, and {210} planes. Although the flake was not free of inclusions, they were avoided in the Brillouin measurements. The crystal was mounted and oriented on a Buerger precession camera using standard techniques. It was then transferred to a four-circle single-crystal diffractometer, and an orientation matrix was computed [*Busing and Levy*, 1967] using a number of high-angle reflections. The cell constants determined from the X-ray work are listed in Table 2. Two orientations were used in making Brillouin measurements. Acoustic velocities in 34 directions were measured with the *c* axis parallel to the spindle axis. The crystal was remounted with *b* parallel to the spindle, and 16 additional directions were measured.

2.2 *Brillouin Measurements*

The apparatus for detecting Brillouin frequency shifts has been described many times [e.g., *Vaughan*, 1979; *Weidner and Carleton*, 1977; *Stoicheff*, 1977; *Weidner et al.*, 1975; *Benedek and Fritsch*, 1966]. and will not be discussed here. Brillouin spectra were obtained with a variety of optical polarizations giving 80 distinct spectra in 48 different crystallographic directions. Acoustic velocities for each of these spectra were calculated by a FORTRAN program (VELOC4), described by *Vaughan and Weidner* [1978], *Vaughan*, [1979], and *Vaughan and Bass* [1983], and listed by *Vaughan*, [1987]. Finally, these velocities were used to calculate the single-crystal elastic moduli using another FORTRAN program (ORTHO8). The algorithms used to determine the elastic moduli are based on the linearized inversion scheme of *Der and Landisman* [1972] and are described by *Weidner and Carleton* [1977]. and listed by M. T. Vaughan and D. J. Weidner (Calculation of single-crystal elastic constants from Brillouin scattering data, part II, Elastic moduli; submitted to *Com-*

[1]Now at Seismological Laboratory, California Institute of Technology, Pasadena.

Paper number 6B6040.
0148-0227/88/006B-6040$05.00

puters and Geosciences, 1987). The moduli are presented in Table 3, and the calculated velocities corresponding to each experimentally determined velocity are presented in Table 4 and illustrated in Figure 1. The rms error in velocity is 35 m/s; the maximum error is 117 m/s. The off-diagonal elements of the trade-off coefficient matrix are close to zero (the maximum value was 0.006 for c_{66} versus c_{12}). This is a good indication of the low interdependence of the individual elastic constants. Finally, the isotropic averages of the elastic moduli for both the Voigt-Reuss and the Hashin-Shtrikman averaging schemes are given in Table 5.

In Figure 1, the experimental and theoretical velocities are shown as a function of crystallographic direction in the (001), (100), and (010) planes. The experimental velocities (symbols) are labeled as in Table 4; the theoretical velocities (solid lines) are derived from the calculated moduli by Christoffel's equation. Theoretical velocities are compared to measured velocities in Table 4. The standard deviations of the moduli (Table 3) are calculated from the rms deviation taking the relative significance of each velocity in determining the moduli into account.

3. DISCUSSION

3.1 *Pyroxene Structure*

Pyroxenes consist of SiO_4 tetrahedra and MO_6 polyhedra in alternating layers parallel to (100). The tetrahedra share corners to form chains parallel to [001] with the base of each tetrahedron approximately in the (100) plane. The polyhedra share edges to form bands also parallel to the c axis. There are two distinct polyhedral sites, M1 and M2. The M1 sites are nearly regular octahedral sites, while the M2 sites are distorted with coordination ranging from six to eight depending on the size of the M2 cation.

When the M2 cation is small as in enstatite, both sites are octahedrally coordinated. The bands of octahedra are separated by voids, and the M2 octahedra are elongated along the b axis. Tetrahedral and octahedral layers are linked by edge sharing between the tetrahedra and the M2 octahedra. The tetrahedral chains kink and the M2 octahedra distort to accommodate the linkage. In addition, the M1 and M2 octahedra share edges. Many of these features are evident in Figure 2, which shows the structure of orthoenstatite viewed down a. A complete discussion of pyroxene topology can be found in the works by Cameron and Papike [1980, 1981].

Pyroxenes of enstatite composition are found in four major polymorphs: high clinoenstatite (space group $C2/c$), low clinoenstatite ($P2_1/c$), orthoenstatite ($Pbca$), and protoenstatite ($Pbcn$) (see *Carlson* [1985] and *Smyth* [1974] for exceptions). Variation among the structure types is primarily the result of differences in stacking of octahedral layers, with differences in the tetrahedral chains also begin important. Octahedral stacking is defined as positive or negative depending on whether the apices of the upper triangular faces of each octahedron point in the $+c$ direction or $-c$ direction. In orthoenstatite the stacking sequence is $++--++\ldots$; whereas stacking in protoenstatite is $+-+-\ldots$; and the monoclinic pyroxenes stack $+++\ldots$ The stacking of polyhedral units along a for the orthoenstatite structure is shown in Figure 3.

Low clinoenstatite and orthoenstatite also differ from other pyroxenes in that they possess two symmetrically distinct tetrahedral chains. The chains differ from each other in kinking angle, distortion, and size of tetrahedra. The kinking angle in pyroxene tetrahedral chains is defined as the angle between the O3-O3-O3 oxygens. An ideal, fully extended chain has an O3-O3-O3 angle of 180°, whereas a fully kinked chain has an O3-O3-O3 angle of 120°. In orthopyroxenes, the tetrahedra of the more kinked chain are larger and share no edges with the M2 octahedra.

The substitution of Fe^{2+} for Mg^{2+} affects the pyroxene structure in several ways. The size of both octahedra increase with iron content, and the M2 site becomes more distorted, while the M1 site remains regular [*Virgo and Hafner*, 1969]. Iron substitution also tends to straighten the tetrahedral chains. In orthopyroxenes, cation site ordering is strong with Mg preferring the M1 site and Fe^{2+} preferring the M2 site [*Ghose*, 1965]. However, the extent of ordering is dependent on thermal history [*Evans et al.*, 1967] and is therefore generally unknown. *Virgo and Hafner* [1969] have shown from Mossbauer spectroscopy that heating of samples can induce disorder. They conclude that crystals from volcanic rocks are likely to retain metastable disorder as a result of rapid cooling, while those from granulite facies metamorphic rocks should exhibit a high degree of order.

3.2 *Structural and Chemical Control of Elasticity*

With this study, the single-crystal elasticity data base for orthopyroxenes expands to six compositions: En_{100} [*Weidner et al.*, 1978], En_{94} (this study), En_{84} [*Kumazawa*, 1969], En_{80} [*Frisillo and Barsch*, 1972, *Webb and Jackson*, 1985], En_0 [*Bass and Weidner*, 1984], and a bronzite of unknown composition [*Ryzhova*

TABLE 1. Chemical Composition

Oxide	Weight Percent
SiO_2	57.47 ± 0.32
MgO	36.33 ± 0.23
FeO	3.86 ± 0.09
Al_2O_3	0.32 ± 0.01
CaO	0.22 ± 0.01
MnO	0.18 ± 0.01
TiO_2	bd.
Cr_2O_3	bd.
Total	98.38 ± 0.40

bd. indicates below detection.

TABLE 2. Unit Cell Parameters

	Value
a	1.8204(1) nm
b	0.8814(1) nm
c	0.5176(1) nm
Volume	0.8304(2) nm^3
X-ray density	3272(2) kg/m^3

Numbers in parentheses indicate estimated standard deviations in the last significant figure.

TABLE 3. Single-Crystal Elastic Constants of Enstatite

Stiffnesses, GPa	Compliances, GPa^{-1}
c_{11} = 229.3 ± 1.1	s_{11} = 0.00520
c_{22} = 167.0 ± 1.1	s_{22} = 0.00723
c_{33} = 193.9 ± 1.5	s_{33} = 0.00566
c_{44} = 79.7 ± 0.7	s_{44} = 0.01253
c_{55} = 76.1 ± 0.6	s_{55} = 0.01314
c_{66} = 77.1 ± 0.8	s_{66} = 0.01297
c_{12} = 73.6 ± 1.7	s_{12} = −0.00206
c_{13} = 49.8 ± 1.6	s_{13} = −0.00084
c_{23} = 46.6 ± 1.6	s_{23} = 0.00121

The uncertainties listed are one standard deviation in the last unit(s) based on an rms deviation of 35 m/s.

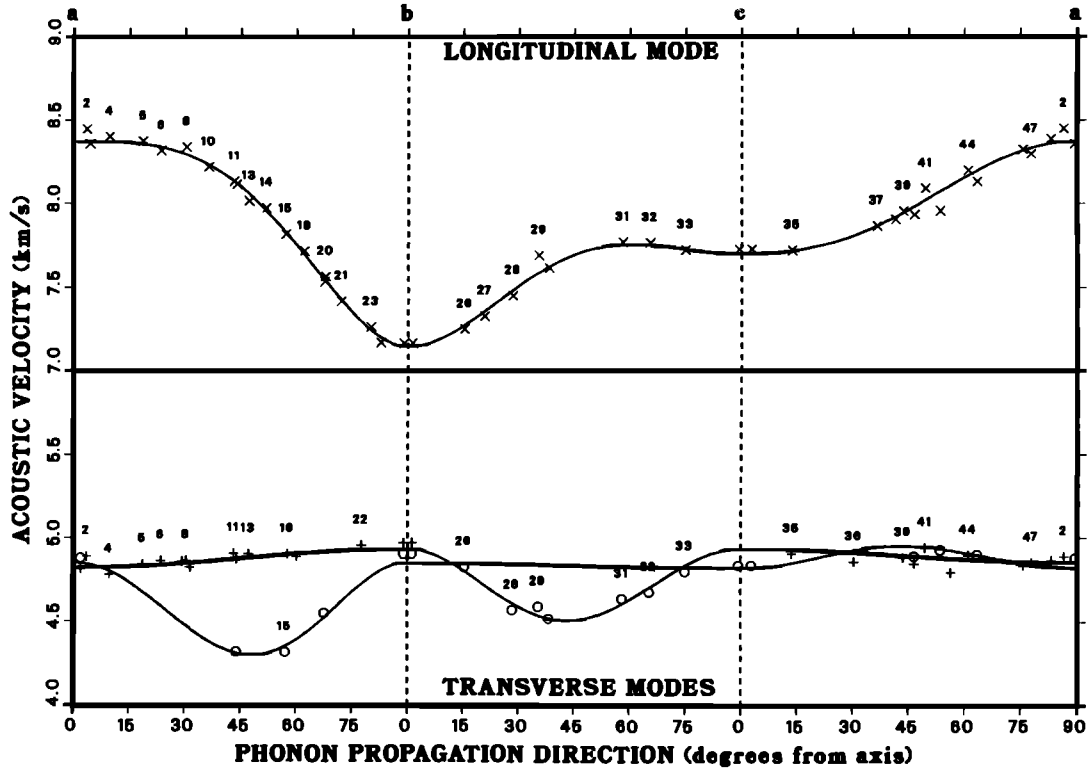

Fig. 1. Acoustic velocities in enstatite. Velocities are plotted as a function of direction in the (001), (100), and (010). Individual data points are labeled to correspond to Table 1. Circles and pluses represent horizontally and vertically polarized shear waves, respectively.

et al., 1966]. Several other pyroxenes have also been characterized including jadeite [*Kandelin and Weidner*, 1987a], hedenbergite [*Kandelin and Weidner*, 1987b], protoenstatite [*Vaughan and Bass*, 1983], germanate orthopyroxene [*Kandelin et al.*, 1983], diopside [*Levien et al.*, 1979], and several additional monoclinic pyroxenes [*Aleksandrov et al.*, 1963; *Aleksandrov and Ryzhova*, 1961]. A number of papers [*Bass and Weidner*, 1984; *Vaughan and Bass*, 1983; *Weidner and Vaughan*, 1982; *Weidner et al.*, 1982] have attempted to relate structural and chemical variations among pyroxenes to their single-crystal elastic properties. This is accomplished by envisioning the structure as composed of a number of elastic units, usually coordination polyhedra. Elastic moduli then depend qualitatively on the stiffness of the polyhedra, their linkages, and their ability to accommodate stress by other means (i.e. rotation).

Table 6 and Figure 4 show the variation of individual elastic stiffnesses as a function of composition for five orthopyroxenes. Figure 4 shows that the individual moduli do not vary systematically between end-members. Most moduli achieve maxima or minima at intermediate compositions. This is in contrast to the way the elastic properties of solid solutions are thought to behave. Although the variation of moduli within solid solutions is poorly understood [*Jackson et al.*, 1978], it is generally assumed that the elastic properties of intermediate compositions are linearly related in some way to the end-member properties. The weighting factors are usually taken to be either mole fractions of end members [*Isaak and Graham*, 1976; *Babuska et al.*, 1978] or molar volumes [*Takahashi and Liu*, 1970].

Empirical evidence from a number of systems supports the general applicability of linear mixing models, particularly for bulk properties [*Jackson et al.*, 1978]. For individual moduli in orthopyroxenes, the evidence clearly does not support such models. However, it may be possible to explain some of these nonsystematic variations by reference to the structural-mechanical model described above.

3.2.1 Modulus c_{11}. The modulus c_{11} is thought to depend strongly on composition [*Weidner and Vaughan*, 1982]. Referring to Figure 3, a stress applied along *a* is normal to layering and should depend on the weakest layer. High-pressure structural studies of pyroxenes have shown that the tetrahedra are less compressable than the octahedra. In addition, the tetrahedra have little rotational freedom in response to a stress in this direction. Therefore it is expected that c_{11} should depend most on the stiffest element in the octahedral layer. Structural studies indicate that this is M1, in keeping with the idea that shorter bonds are stronger bonds. The modulus c_{11} should then directly reflect the composition of the M1 site. Such a conclusion is reinforced by the linear relationship observed between average M1-O bond distance (‹M1-O›) and c_{11} for pyroxenes of different structures and compositions [*Bass and Weidner*, 1984]. The small variability of c_{11} for all pyroxenes is taken as evidence that structural controls are more important than chemical variations in defining pyroxene elasticity [*Weidner and Vaughan*, 1982]. The small variability of c_{11} for orthopyroxenes in the compositional range En_{80}-En_{100} is believed to be consistent with a model of ordered substitution of Fe^{2+} into the M2 site [*Bass and Weidner*, 1984].

3.2.2 Effect of ordering. If one assumes complete ordering of iron and magnesium in the octahedral sites and if one assumes that c_{11} and c_{22} are controlled by M1 and M2, then an alternative interpretation is that between En_{100} and En_{50}, iron should go into the M2 site; therefore M1 and hence c_{11} should remain constant. However, c_{22} should decrease with increasing iron content because it is dependent on M2, and Fe-containing octahedra are more compressable than Mg-containing octahedra. At En_{50}, M2 is

TABLE 4. Acoustic Velocities Determined for Enstatite

	Direction			Compressional			Shear V			Shear H		
No.	X	Y	Z	Obser.	Calc.	Diff.	Obser.	Calc.	Diff.	Obser.	Calc.	Diff.
1	−0.999	0.034	0.010	—	8372	—	4815	4821	−6	4881	4853	29
2	−0.998	0.018	−0.060	8447	8369	79	4892	4854	37	—	4823	—
3	0.997	−0.078	−0.010	8357	8372	−15	—	4822	—	—	4843	—
4	0.986	0.169	−0.006	8401	8369	32	4783	4824	−41	—	4803	—
5	−0.947	−0.321	0.004	8373	8356	18	4845	4833	12	—	4679	—
6	0.916	−0.401	0.003	8316	8337	−21	4865	4840	25	—	4593	—
7	−0.872	−0.490	0.001	—	8301	—	4861	4849	12	—	4492	—
8	−0.862	0.507	0.015	8338	8292	46	4866	4851	15	—	4473	—
9	0.853	−0.522	−0.015	—	8282	—	4825	4853	−27	—	4456	—
10	0.805	−0.593	−0.016	8218	8231	−13	—	4862	—	—	4385	—
11	0.729	−0.684	−0.016	8130	8131	−1	4909	4876	34	—	4317	—
12	0.720	0.694	0.003	8112	8117	−5	4873	4877	−4	4319	4313	7
13	−0.678	−0.735	−0.005	8013	8055	−42	4906	4883	23	—	4302	—
14	0.616	−0.788	−0.016	7972	7954	18	—	4893	—	—	4310	—
15	0.542	−0.840	−0.017	7816	7828	−11	—	4903	—	4318	4352	−34
16	−0.532	−0.846	−0.007	—	7811	—	4906	4904	3	—	4359	—
17	0.496	−0.868	−0.017	—	7746	—	4891	4908	−17	—	4391	—
18	−0.465	0.885	0.017	7714	7693	21	—	4911	—	—	4422	—
19	−0.379	−0.925	−0.010	7532	7543	−11	—	4920	—	4552	4523	29
20	−0.375	−0.927	−0.010	7562	7537	25	—	4920	—	—	4528	—
21	−0.307	−0.952	−0.011	7416	7425	−9	—	4925	—	—	4614	—
22	−0.214	0.977	0.016	—	7291	—	4958	4931	27	—	4725	—
23	0.172	0.985	0.013	7264	7242	22	—	4933	—	—	4768	—
24	0.126	0.992	0.013	7169	7198	−29	—	4934	—	—	4807	—
25	−0.017	−1.000	−0.014	7165	7146	19	4973	4935	37	4907	4853	54
26	0.014	0.964	0.265	7250	7274	−23	4828	4804	24	—	4854	—
27	0.026	0.935	−0.354	7330	7360	−30	—	4720	—	—	4852	—
28	0.006	0.879	−0.476	7450	7484	−34	4572	4612	−40	—	4847	—
29	0.026	0.814	0.580	7690	7588	101	4593	4539	54	—	4844	—
30	0.012	0.785	−0.620	7616	7624	−8	4520	4522	−2	—	4842	—
31	−0.049	−0.529	0.847	7768	7755	13	4638	4605	34	—	4833	—
32	−0.069	−0.415	0.907	7763	7753	11	4677	4702	−25	—	4831	—
33	−0.046	−0.259	0.965	7721	7727	−6	4800	4837	−37	—	4822	—
34	−0.048	−0.011	0.999	7725	7699	26	—	4936	—	4837	4822	15
35	0.234	0.028	0.972	7720	7717	3	4908	4930	−22	—	4851	—
36	0.506	0.008	0.863	—	7809	—	4861	4915	−54	—	4929	—
37	0.595	0.008	0.804	7863	7865	−2	—	4907	—	—	4947	—
38	0.661	0.007	0.750	7903	7918	−15	—	4900	—	—	4954	—
39	−0.689	0.019	0.724	7951	7944	7	4886	4897	−11	—	4955	—
40	0.726	0.006	0.688	7932	7980	−49	4850	4893	−44	4893	4953	−59
41	0.760	−0.007	−0.650	8087	8017	70	4945	4948	−3	—	4889	—
42	−0.804	0.008	0.595	7953	8070	−117	—	4884	—	4929	4938	−9
43	0.832	0.004	0.554	—	8107	—	4797	4880	−83	—	4928	—
44	0.875	−0.026	0.484	8197	8167	31	4899	4909	−10	—	4873	—
45	−0.893	−0.050	0.448	8128	8195	−67	—	4867	—	4903	4900	3
46	−0.978	0.004	0.210	8294	8332	−38	4855	4858	−3	—	4841	—
47	0.969	−0.014	0.248	8323	8316	6	4838	4848	−10	—	4859	—
48	0.993	−0.025	0.119	8383	8359	24	4869	4827	41	—	4855	—

The rms error = 35 m/s. Reference number refers to the acoustic direction and corresponds to the data point numbers in Figure 1. Directions are the direction cosines of the wave normal of the particular acoustic wave, relative to the IRE orthonormal crystallographic coordinates (*X* parallel to *a**, *Y* parallel to *b**, and *Z* parallel to *c*). The three sets of three columns each are the velocities of the compressional and two shear modes, in meters per second. The displacement of the vertical shear mode is approximately (0,0,1) for directions 1–24, (1,0,0) for directions 25–34,and (0,1,0) for directions 35–48.

filled with iron and any additional iron must enter M1; therefore c_{22} should now remain constant, while c_{11} should now decrease with increasing iron content. This is shown in Figure 5.

3.2.3 Modulus c_{33}. The modulus c_{33} is the most variable of the longitudinal moduli. According to our model, it should depend on the chains of tetrahedra running along *c* [*Weidner and Vaughan*, 1982]. The stiffness of the tetrahedral chains is believed to depend on their rotational freedom as measured by the kinking angle. The inconsistency of some of the experimental data with this interpretation led to the modification that there is some angle of kinking below which the tetrahedral chains become passive and the octahedral bands support the strain [*Vaughan and Bass*, 1983]. The notion of some compositional influence over c_{33} is supported by the nearly linear decrease of c_{33} with composition found by *Bass and Weidner* [1984].

The most anomalous elastic constant measured in this study is also c_{33}: it decreases 12% between En_{100} and En_{94} and increases 6% between En_{94} and En_{84}. While the overall trend for c_{33} is to decrease with increasing iron content, it undergoes a sharp linear increase with iron in the range En_{94}-En_{80}. The results of this study suggest that c_{33} cannot be related to composition in any simple systematic way.

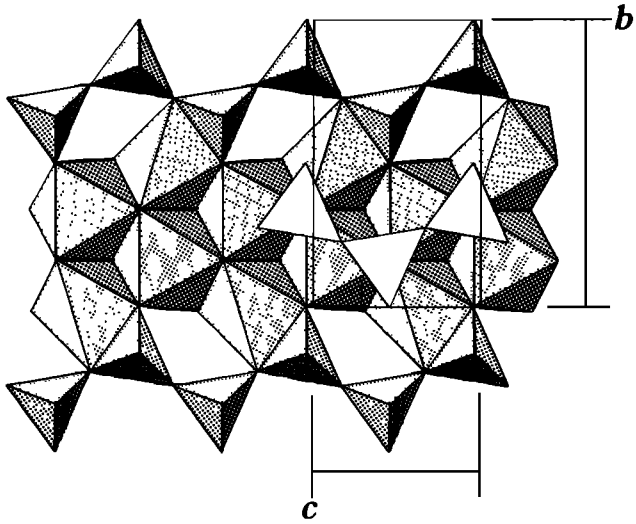

Fig. 2. Projection of orthoenstatite onto the (100) plane. The octahedra form wide bands, and the tetrahedra form chains along [001]. The larger, distorted M2 octahedra share edges with tetrahedra; the M1 octahedra share corners with tetrahedra. Also shown are the voids in the octahedral layer.

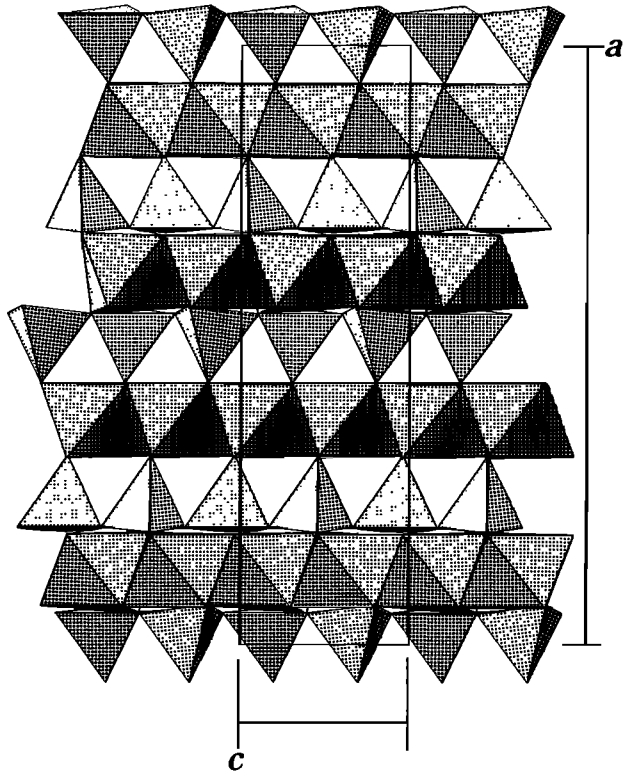

Fig. 3. Orthoenstatite structure viewed down [010]. Tetrahedra and octahedra are arranged in alternating layers along [100].

3.2.4 Comparison of c_{11} with c_{33}. For all orthopyroxenes c_{11} is greater than c_{33} while for such other pyroxenes as protoenstatite, diopside, and jadeite, c_{11} is less than c_{33}. It is interesting to note that all pyroxenes in the latter group have one symmetrically distinct tetrahedral chain, while orthopyroxenes have two. This rule holds for structures exhibiting a wide range of kinking angles. For example, kinking angles in diopside and ferrosilite differ by only a few degrees, yet c_{33} for diopside is greater by about 33%. The explanation for this lies in the fact that one of the tetrahedral chains in orthopyroxenes is more kinked than the other. This chain is weaker, and when stress is applied along the c direction, it can be expected to be passive. The strain must then be distributed among a smaller number of structural units, and consequently, the modulus is lowered in value.

3.2.5 Modulus c_{22}. The response to stress along b is controlled by c_{22}. For protoenstatite, where Li^+ is ordered on the M2 site, c_{22} is very low suggesting significant M2 compositional control [*Vaughan and Bass*, 1983]. *Bass and Weidner* [1984] concluded that for compositions greater than En_{80}, the decrease of c_{22} is substantially greater than a linear trend would indicate. They claimed that this observation supported the idea of strong ordering of Fe^{2+} on the M2 site.

With the new data acquired in this study, it appears that c_{22} displays a greater than linear increase with increasing iron content only for compositions above En_{94}. Between En_{94} and En_0, there is little difference between the slopes of c_{11} and c_{22}. The curves do differ in that c_{11} appears to vary more smoothly than c_{22}. This is consistent with the view that variations in site ordering result in localized changes in c_{22}, but the overall trend for this modulus is very similar to c_{11}.

For all pyroxenes studied to date, c_{22} is the lowest of the longitudinal moduli. This has been attributed in part to the relative ease of rotation in this direction and the overall weakness of the M2 site [*Weidner and Vaughan*, 1982]. It has also been proposed that voids in the b-c plane lower the value of c_{22} [*Vaughan and Bass*, 1983]. However, the data do not support this last idea. When large cations occupy the M2 site, the voids in the structure are filled in [*Cameron and Papike*, 1980, 1981]. If the voids were significant, c_{22} for diopside would be much greater than c_{22} for orthoenstatite. In fact, c_{22} for diopside is slightly less than c_{22} for orthoenstatite. Furthermore, the voids apparently do not have much affect on shear in the b-c plane since c_{44} is the largest of the shear moduli. Thus existing evidence does not support the role of structural voids in contributing to c_{22}. A possibility that has not been considered, however, is that the distortion of the M2 polyhedra can help explain the low value of the modulus. Structural studies indicate that M2 is only slightly less stiff than M1 [*Bass and Weidner*,

TABLE 5. Calculated and Measured Isotropic Elastic Moduli and Acoustic Velocities

	Reuss	HS−	VRH Average	HS+	Voigt
Bulk modulus, GPa	101.2	102.0	102.3	102.4	103.3
Shear modulus, GPa	73.2	73.8	73.9	74.0	74.6
Compressional velocity, m/s	7795	7826	7834	7839	7872
Bulk sound velocity, m/s	5561	5583	5592	5594	5619
Shear velocity, m/s	4730	4749	4752	4756	4775

Hashin-Shtrikman (HS) bounds based on *Watt*[1979, 1987].

TABLE 6. Comparison of Pyroxene Elastic Properties

	En_{100}	En_{94}	En_{84}	En_{80}	En_0	PEN	DI
c_{11}	224.7	229.3	229.9	228.6	198	219	223
c_{22}	177.9	167.0	165.4	160.5	136	160	171
c_{33}	213.6	193.9	205.7	210.4	175	242	235
c_{44}	77.6	79.7	83.1	81.8	59	87	74
c_{55}	75.9	76.1	76.4	75.5	58	45	67
c_{66}	81.6	77.1	79.5	77.6	49	66	66
c_{12}	72.4	73.6	70.1	71.0	84	87	77
c_{13}	54.1	49.8	57.3	54.8	72	39	81
c_{23}	52.7	46.6	49.6	46.0	55	42	57
$<c_{11}>$	205.4	196.7	200.3	199.8	170	207	210
$<c_{44}>$	78.4	77.6	79.7	78.3	69	66	69
$<c_{12}>$	59.7	56.7	59.0	57.3	70	59	72
K(VRH)	107.8	102.3	105.0	103.5	101	116	106
G(VRH)	75.7	73.9	75.0	75.5	52	63	67
O3–O3–O3, deg	158.9, 139.0	159.6, 139.5	160.6, 140.1	161.0, 140.3	169.1, 143.8	167.3	166.4

PEN is Mg–rich Li–Sc protopyroxene; DI is diopside. References for elasticity data are given in text; O3–O3–O3 kinking angle from *Cameron and Papike* [1981]. Intermediate orthopyroxene values are interpolated.

1984], but because they are elongated along *b*, the M2 octahedra may be much more compressable in that direction.

3.2.6 Shear moduli. Due to the complexity of the pyroxene structure, structural and chemical controls of the shear moduli are more difficult to isolate. Nevertheless, some trends in the data are apparent. The shear moduli c_{55} and c_{66} have been found to be related to octahedral stacking along *a* [*Vaughan and Bass*, 1983]. The small variability of all three shear moduli for Mg-rich compositions is taken as further evidence for strong control by site ordering [*Bass and Weidner*, 1984]. Figure 4 shows that the shear moduli behave in a broadly similar way in the compositional range En_{94}-En_{80}: all vary nonsystematically, achieving local maxima at En_{84}. If these variations are the result of order-disorder phenomena, then it is significant that the influence of site ordering is the same on each shear modulus. It should also be noted that there is no systematic behavior for the shear moduli above En_{94}. Overall, c_{55} shows the least compositional variation and is consistent with the interpretation of structural control. The modulus c_{44} shows primarily compositional control. For almost all pyroxenes, c_{44} is the largest of the shear moduli. This can be related to the inability of the polyhedral elements to take up the applied stress by rotating out of the *b-c* plane. The fact that c_{44} is generally not much greater than the other shear moduli could indicate that this is not a major control of elasticity. Finally, c_{66} appears to be sensitive to both structure and composition.

3.2.7 Off-diagonal moduli. The off-diagonal moduli (c_{12}, c_{13},

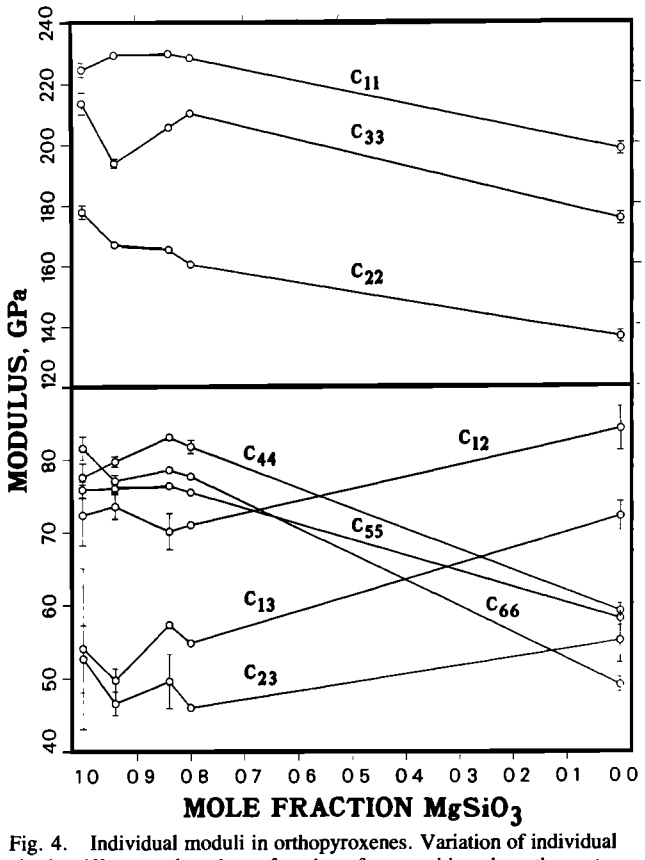

Fig. 4. Individual moduli in orthopyroxenes. Variation of individual elastic stiffnesses plotted as a function of composition along the enstatite-ferrosilite join. Error bars correspond to one standard deviation in the moduli and are within the circles if not shown. The data points are En_{100} [*Weidner et al.*, 1978]; En_{94} (this work); En_{84} [*Kumazawa*, 1969]; En_{80} [*Frisillo and Barsch*, 1972]; and En_0 [*Bass and Weidner*, [1984].

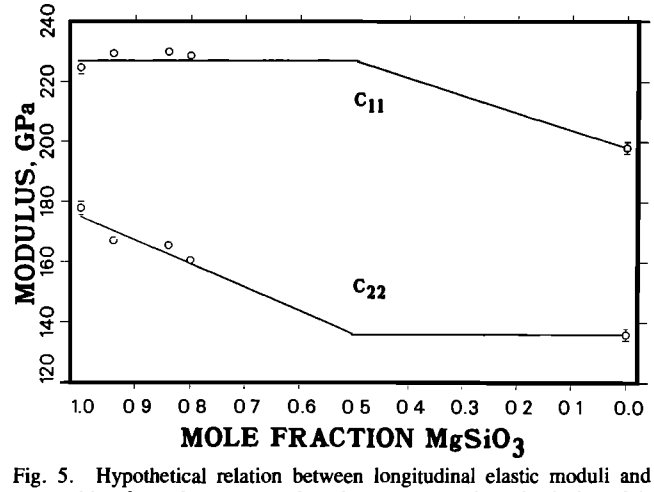

Fig. 5. Hypothetical relation between longitudinal elastic moduli and composition for orthopyroxenes based on a structural mechanical model. Assumptions are that the intermediate composition minerals are fully ordered with respect to magnesium and iron in M2 and M1, respectively. Modified from *Vaughan* [1986].

and c_{23}) are even more difficult to interpret because of the greater complexity of the forces that govern them and the larger error bars in the data. Normally, the off-diagonal moduli of the pyroxenes are the least variable. Table 6 indicates that c_{12} and c_{23} vary little with either structure or composition. On the other hand, c_{13} shows little compositional variation but can show a great deal of structural variation. This modulus then is probably related to the stacking of the octahedral layers. It should also be noted that between En_{94} and En_{80}, c_{13} and c_{23} behave similarly to the shear moduli, with local maxima at En_{84}. The opposite behavior is observed for c_{12}, which achieves a minimum at En_{84}. Thus it is possible that the nonsystematic behavior of all these moduli may have the same underlying cause.

The off-diagonal moduli are unique in that they increase with iron content. This has been attributed to fundamental differences between transition-metal and alkaline-Earth cations [*Weidner et al.*, 1982]. The relative magnitudes of the moduli can be explained with reference to our model. In general, the off-diagonal moduli represent the resistance to expansion in a direction normal to applied stress (Table 2). c_{23} and c_{13} are low relative to c_{12} because the structure can expand relatively easily along the c direction by straightening of the tetrahedral chains. Conversely, there is no easy way for the structure to expand normal to c.

3.2.8 Averaged moduli. Figure 6 shows a plot of the averaged moduli $\langle c_{11}\rangle$, $\langle c_{44}\rangle$, and $\langle c_{12}\rangle$ as functions of composition, (where $\langle c_{11}\rangle$ is the average of c_{11}, c_{22}, and c_{33}; $\langle c_{44}\rangle$ is the average of c_{44}, c_{55}, and c_{66}; and $\langle c_{12}\rangle$ is the average of c_{12}, c_{13}, and c_{23}). The low variability of $\langle c_{12}\rangle$ and $\langle c_{44}\rangle$ at low Fe concentrations has been attributed to site ordering [*Bass and Weidner*, 1984]. The results of this study concur with the notion that variation in $\langle c_{44}\rangle$ is strongly damped at concentrations of greater than 80% Mg. However, our results suggest that $\langle c_{12}\rangle$ is best described by a linear increase with decreasing enstatite content. The off-diagonal moduli tend to vary little from one pyroxene to the next, as discussed above. With this study, nonsystematic variations in $\langle c_{11}\rangle$ become apparent for the first time, largely as a result of the low value of c_{33}. This is in sharp contrast to the olivine system where the behavior of all three averaged moduli is approximately linear [*Yeganeh-Haeri and Vaughan*, 1984].

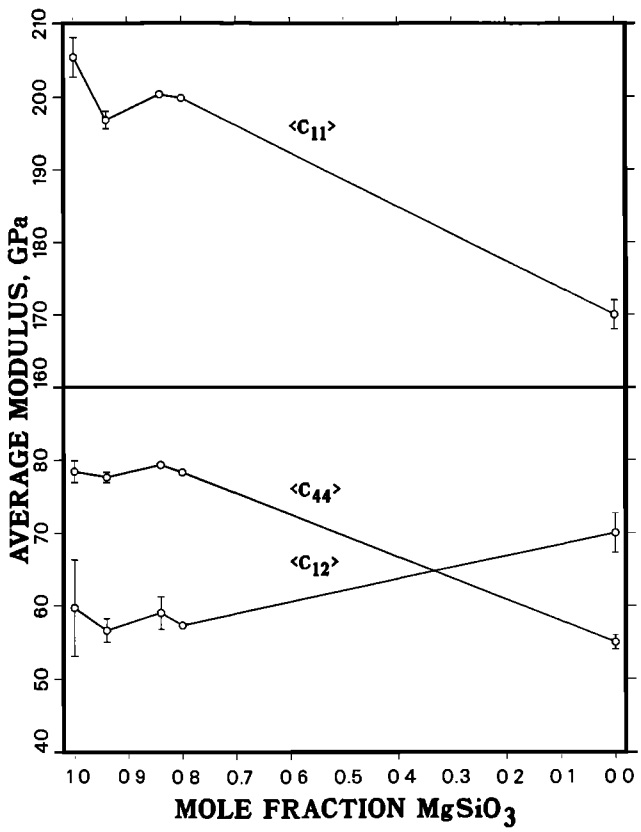

Fig. 6. Average moduli *vs.* composition for orthopyroxenes. Data points are the same as in Figure 4.

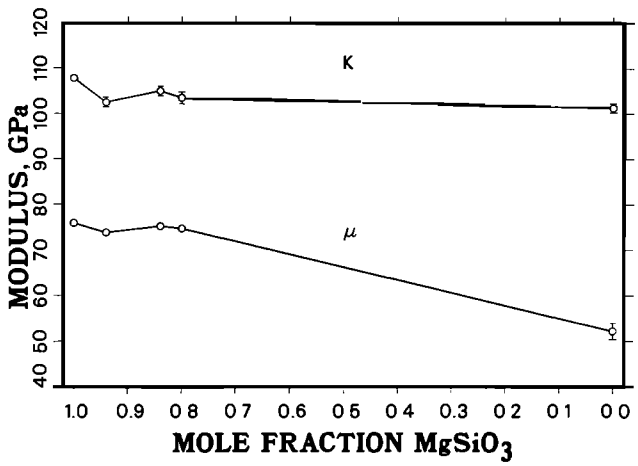

Fig. 7. Aggregate Moduli of Orthopyroxenes. Bulk (K) and shear (μ) moduli (VRH averages) of orthopyroxenes of figure 6. Error bars indicate the Voigt and Reuss bounds of the moduli but do not indicate the uncertainties in those bounds.

The Voigt-Reuss-Hill (VRH) averages for the bulk and shear moduli derived from the single-crystal data are shown in Figure 7. The bulk modulus K_S measured in this work is consistent with the interpretation that K_S depends only on crystal structure and is independent of composition [*Bass and Weidner*, 1984; *Anderson*, 1976; *Jackson et al.*, 1978]. Our bulk modulus is 5% lower than that measured for pure orthoenstatite by *Weidner et al.* [1978]. The difference is largely due to our lower values of c_{22} and c_{33} and to differences in $\langle c_{12}\rangle$. The value of $\langle c_{12}\rangle$ measured by Weidner *et al.* is uncertain. The results of this study, together with the results from the bronzites, suggest that their value may be overestimated, although certainly within reported uncertainties. Thus we feel that our result is a better estimate of the bulk modulus for enstatite composition orthopyroxenes.

Previously measured shear moduli for compositions greater than 0.8 mole fraction enstatite have been found to be nearly constant. This has been explained as a consequence of site preferences [*Bass and Weidner*, 1984]. The value obtained in this study, however, is most consistent with a linear increase with decreasing enstatite content. This discrepancy could merely be a reflection of differences between samples. For example, if the bronzites of *Kumazawa* [1969] and *Frisillo and Barsch* [1972] are highly ordered and our sample is disordered, then the observed behavior is exactly as expected. Better crystallographic characterization of samples could help settle this issue.

The nonlinear variations in moduli evident in Figures 4, 6, and 7 might be attributable to differences in the various experimental techniques. However, the elastic constants measured here are generally more consistent with the ultrasonic data of *Kumazawa* [1969] than with the Brillouin data of *Weidner et al.* [1978]. Furthermore, ultrasonics and Brillouin scattering have been shown to give similar results [*Vaughan et al.*, 1981; *Weidner et al.*, 1978]. Thus it does not seem likely that experimental differences can explain the resulting complex variation. The role of impurities has

been discussed above and can be considered to be minor because the quantity of impurities is small. The best explanation for the nonsystematic behavior is that it represents the sum of sample-to-sample variations in such factors as cation site ordering. The unusual behavior between En_{94} and En_{100} probably cannot be explained by small differences in chemistry, however. These discrepancies may reflect intrinsic differences between the elastic behavior of natural and synthetic samples. On the other hand, the differences may be due to the limitations of the data set of *Weidner et al.* [1978]. Among the problems with their data is that they made no explicit corrections for the effect of refraction at crystal faces, nor did they account for the variation of refractive index in the incident and scattered directions. However, these errors are likely to be small because of the low refractive index and birefringence of orthoenstatite. Furthermore, they measured fewer velocities which were not as well distributed as the velocities measured in this study. A useful step in resolving some of the problems discussed above would be to remeasure the elastic constants of pure orthoenstatite.

4. CONCLUSIONS

Brillouin scattering has been used to measure the single-crystal elastic constants of an orthopyroxene of enstatite composition at 20°C and 1 bar. The new data have been compared with extant single-crystal pyroxene elasticity data, and previously identified nonsystematic behavior is confirmed. Some of this behavior can be qualitatively related to crystal structure and composition on the basis of a structural-mechanical model.

The longitudinal moduli tend to be more variable than the others. The moduli c_{11} and c_{22} are primarily related to the composition of the octahedral sites. The modulus c_{11} for intermediate composition orthopyroxenes is found to deviate from the observed linear relationship with ‹M1-O›. This is attributed to the effects of both site ordering and impurities. The modulus c_{22} shows near linear variation over greater than 90% of the compositional range of orthopyroxenes. The modulus c_{33} displays a very pronounced minimum at En_{94} which could not be explained by any structural or chemical features. We do note, however, that the magnitude of c_{33} relative to c_{11} is well correlated with the number of distinct tetrahedral chains.

The shear and off-diagonal moduli, although nonsystematic, tend to vary in similar ways, as most moduli achieve local minima or maxima at En_{84}. This is believed to be a reflection of small-scale sample-to-sample variabilities. For low Fe concentrations, the behavior of the shear moduli is best explained by ordered cation substitution. The low variability of the off-diagonal moduli, however, is probably a basic feature of the pyroxene structure.

Among the averaged moduli, nonsystematic variation in $\langle c_{11} \rangle$ is apparent for the first time with this study. It is caused by the unusual behavior of c_{33}. The averaged shear modulus, $\langle c_{44} \rangle$, reflects order-disorder phenomena as discussed above; and $\langle c_{12} \rangle$ is consistent with a linear rate of decrease between end-members.

The shear modulus, m, measured here appears to vary linearly with composition. The bulk modulus is essentially constant for all orthopyroxenes. Our value for the bulk modulus is 5% lower than that measured by *Weidner et al.* [1978]. We believe that ours is a better value because the individual constants are more tightly constrained. In many cases our data define a different trend than that suggested by the data for the Mg-rich end-member. It may be possible to resolve these discrepancies by remeasuring the elastic constants of pure orthoenstatite. In addition, it may be possible to answer questions about some individual moduli (c_{11} and c_{33}, for example) and about the effects of site ordering by better crystallographic characterization of the sample used in this study and by additional measurements on well characterized samples in a wider compositional range, especially En_0 to En_{80}.

Acknowledgments. W. Baur and M. Flower are gratefully acknowledged for their many helpful comments and suggestions. Special thanks are extended to S. Guggenheim for his assistance with the X-ray work associated with this project. G. Harris assisted in the sample preparation process and his help is greatly appreciated. J. Walther of Northwestern University kindly made that Univesity's microprobe available for sample analysis. R. Fischer supplied an advanced version of his crystal structure plotting program, STRUPLO84 (Fischer, 1985). J. Peter Watt provided the FORTRAN program used to calculate the Hashin-Shtrikman bounds on the polycrystalline elastic moduli (Watt, 1987). Reviews by J. D. Bass and D. J. Weidner were very helpful. This research was supported in part by the National Science Foundation under grants EAR 82-12748 to M. Vaughan and S. Guggenheim. and EAR 86-18616 to M. Vaughan.

REFERENCES

Aleksandrov, K. S., and T. V. Ryzhova, The elastic properties of rock forming minerals, 1, Pyroxenes and amphiboles, *Izv. Acad. Sci. USSR Phys. Solid Earth*, Engl. Transl., *1961*, 871–875, 1961.

Aleksandrov, K. S., T. V. Ryzhova, and B. P. Belikov, The elastic properties of pyroxenes, *Sov. Phys. Crystallog.*, *8*, 589–591, 1963.

Babuska, V., J. Fiala, M. Kumazawa, I. Ohno, and Y. Sumino, Elastic properties of garnet solid solution series, *Phys. Earth Planet. Inter.*, *16*, 157–176, 1978.

Bass, J. D., and D. L. Anderson, Composition of the upper mantle: Geophysical tests of two petrological models, *Geophys. Res. Lett.*, *11*, 237–240, 1984.

Bass, J. D., and D. J. Weidner, Elasticity of single-crystal orthoferrosilite, *J. Geophys. Res.*, *89*, 4359-4372, 1984.

Benedek, G. B., and K. Fritsch, Brillouin scattering in cubic crystals, *Phys. Rev.*, *149*, 647–662, 1966.

Busing, W. R., and H. A. Levy, Angle calculations for 3- and 4-circle X-ray and neutron diffractometers, *Acta Crystallog.*, *22*, 457-464, 1967.

Cameron, M., and J. J. Papike, Crystal chemistry of silicate pyroxenes, in *Pyroxenes, Rev. Mineral.*, vol. 7, edited by C. T. Prewitt, pp. 5–92, Mineralogical Society of America, Washington, D. C., 1980.

Cameron, M., and J. J. Papike, Structural and chemical variations in pyroxenes, *Am. Mineral.*, *66*, 1–50, 1981.

Carlson, W. D., Evidence against the stability of orthoenstatite above 1005° C at atmospheric pressure in CaO-MgO-SiO_2, *Geophys. Res. Lett.*, *7*, 409–411, 1985.

Der, S. A., and M. Landisman, Theory for errors, resolution, and separation of unknown variables in inverse problems, with application to the mantle and crust in southern Africa and Scandinavia, *Geophys. J. Roy. Astron. Soc.*, *27*, 137–177, 1972.

Evans, B. J., S. Ghose, and S. Hafner, Hyperfine splitting of ^{57}Fe and Mg-Fe disorder in orthopyroxene ($MgSiO_3$-$FeSiO_3$) solid solutions. *J. Geol.*, *75*, 306–322, 1967.

Fischer, R. X., STRUPLO84, a FORTRAN plot program for crystal structure illustrations in polyhedral representation, *J. Appl. Crystallog.*, *18*, 258–262, 1985.

Frisillo, A. L., and G. R. Barsch, Measurement of single-crystal elastic constants of bronzite as a function of pressure and temperature, *J. Geophys. Res.*, *77*, 6366–6384, 1972.

Ghose, S., Mg^{2+}-Fe^{2+} order in an orthopyroxene, $Mg_{0.93}Fe_{1.07}Si_2O_6$, *Z. Kristallogr.*, *122*, 81–99, 1965.

Isaak, D. G., and E. K. Graham, Elastic properties of an almandine–spessartine garnet and elasticity in the garnet solid solution series, *J. Geophys. Res.*, *81*, 1483–2489, 1976.

Jackson, I., R. C. Liebermann, and A. E. Ringwood, The elastic properties of $(Mg_x,Fe_{1-x})O$ solid solutions, *Phys. Chem. Mineral.*, *3*, 11–31, 1978.

Kandelin, J., D. J. Weidner, M. Ozima, and S. Akimoto, Elasticity of germanate and silicate orthopyroxenes (abstract), *EØS Trans. AGU*, *64*, 315, 1983.

Kandelin, J., and D. J. Weidner, The single-crystal elastic properties of jadeite, *Phys Earth Planet. Inter.*, in press, 1987a.

Kandelin, J., and D. J. Weidner, Elastic properties of hedenbergite, *J. Geophys. Res.*, in press, 1987b.

Kumazawa, M., The elastic constants of single-crystal orthopyroxene, *J. Geophys. Res.*, *74*, 5973–5980, 1969.

Levien, L., D. J. Weidner, and C. T. Prewitt, Elasticity of diopside, *Phys. Chem. Mineral.*, *4*, 105–113, 1979.

Ryzhova, T.V., K.S. Aleksandrov, and V.M. Korobkova, The elastic properties of rock-forming minerals, 5, Additional data on silicates, *Izv. Acad. Sci. USSR Phys. Solid Earth*, Engl. Transl., *1966(2)*, 111–113, 1966.

Smyth, J. R., Low orthopyroxene from a lunar deep crustal rock: A new pyroxene polymorph of space group $P2_1ca$, *Geophys. Res. Lett.*, *1*, 27–29, 1974.

Stoicheff, B. P., Brillouin spectroscopy and elastic constants, in *Rare Gas Solids*, vol. 2, edited by M. L. Klein and J. A. Venable, pp. 979–1020, Academic, Orlando, Fla., 1977.

Takahashi, T., and L. Liu, Compression of ferromagnesian garnets and the effect of solid solutions on the bulk modulus, *J. Geophys. Res.*, *75*, 5757–5766, 1970.

Vaughan, M. T., Elasticity and crystal structure in aluminosilicates and pyroxenes, Ph. D. thesis, State Univ. of N. Y. at Stony Brook, Stony Brook, 1979.

Vaughan, M. T., Elasticity and crystal structure (abstract), *EØS Trans. AGU*, *67*, 357, 1986.

Vaughan, M. T.,: Calculation of single-crystal elastic constants from Brillouin scattering data, part I, Acoustic velocities, *Comput. and Geosci.*, in press, 1987.

Vaughan, M. T., and J. D. Bass, Single crystal elastic properties of protoenstatite: A comparison with orthoenstatite, *Phys. Chem. Mineral.*, *10*, 62–68, 1983.

Vaughan, M. T., and D. J. Weidner, The relationship of elasticity and crystal structure in andalusite and silimanite, *Phys. Chem. Mineral.*, *3*, 133–144, 1978.

Vaughan, M. T., M. H. Manghnani, and T. Matsui, Single-crystal elastic constants of pure forsterite: A comparison of ultrasonic and Brillouin scattering data (abstract), *EØS Trans. AGU*, *62*, 392, 1981.

Virgo, D., and S. S. Hafner, Fe^{2+}, Mg order-disorder in heated orthopyroxenes, Spec. Pap. 2, pp. 67–82, Mineral. Soc. of Am., Washington, D. C., 1969.

Webb, S. L., and I. Jackson, The anomalous pressure dependence of the elastic moduli of single-crystal orthopyroxene (abstract), *EØS Trans. AGU*, *66*, 371, 1985.

Watt, J. P., POLYXSTL: A FORTRAN program to calculate average elastic properties of minerals from single-crystal elasticitry data, *Comput. Geosci.*, in press, 1987.

Weidner, D. J., A mineral physics test of a pyrolite mantle, *Geophys. Res. Lett*, *12*, 417–420, 1985.

Weidner, D. J., and H. R. Carleton, Elasticity of coesite, *J. Geophys. Res.*, *82*, 1334–1346, 1977.

Weidner, D. J., and M. T. Vaughan, Elasticity of pyroxenes: Effects of composition versus crystal structure, *J. Geophys. Res.*, *87*, 9349–9353, 1982.

Weidner, D. J., K. Swyler, and H. R. Carleton, Elasticity of microcrystals, *Geophys. Res. Lett.*, *2*, 189–192, 1975.

Weidner, D. J., H. Wang, and J. Ito, Elasticity of orthoenstatite, *Phys. Earth Planet. Inter.*, *17*, P7–P13, 1978.

Weidner, D. J., J. D. Bass, and M. T. Vaughan, The effect of crystal structure and composition on elastic properties of silicates, in *High Pressure Research in Geophysics*, edited by S. Akimoto and M. Manghnani, pp. 125-133, D. Reidel, Hingham, Mass., 1982.

Yeganeh-Haeri, A., and M. T. Vaughan, Single-crystal elastic constants of olivine (abstract), *EØS Trans. AGU*, *65*, 282, 1984.

T. S. Duffy, Seismological Laboratory, California Institute of Technology, Pasadena, Ca 91125

M. T. Vaughan, Department of Geological Sciences (M/C 186), Department of Geological Sciences, University of Illinois at Chicago, Box 4348, Chicago, IL 60680

(Received April 23, 1986;
revised April 23, 1986;
accepted July 29, 1986.)